



# CHORUS

This is the accepted manuscript made available via CHORUS. The article has been published as:

## Heat-transport mechanisms in molecular building blocks of inorganic/organic hybrid superlattices

Ashutosh Giri, Janne-Petteri Niemelä, Tommi Tynell, John T. Gaskins, Brian F. Donovan, Maarit Karppinen, and Patrick E. Hopkins

Phys. Rev. B **93**, 115310 — Published 16 March 2016

DOI: [10.1103/PhysRevB.93.115310](https://doi.org/10.1103/PhysRevB.93.115310)

1 **Heat-transport mechanisms in molecular building blocks of**  
2 **inorganic/organic hybrid superlattices**

3 Ashutosh Giri,<sup>1</sup> Janne-Petteri Niemelä,<sup>2</sup> Tommi Tynell,<sup>2</sup> John T. Gaskins,<sup>1</sup>  
4 Brian F. Donovan,<sup>1</sup> Maarit Karppinen,<sup>2</sup> and Patrick E. Hopkins<sup>1,\*</sup>

5 *<sup>1</sup>Department of Mechanical and Aerospace Engineering,*

6 *University of Virginia, Charlottesville, Virginia 22904, USA*

7 *<sup>2</sup>Department of Chemistry, Aalto University, FI-00076 Aalto, Finland*

8 (Dated: February 19, 2016)

## Abstract

9  
10 Nanomaterial interfaces and concomitant thermal resistances are generally considered as atomic-  
11 scale planes that scatter the fundamental energy carriers. Given that the nanoscale structural and  
12 chemical properties of solid interfaces can strongly influence this thermal boundary conductance,  
13 the ballistic and diffusive nature of phonon transport along with the corresponding phonon wave-  
14 lengths can affect how energy is scattered and transmitted across an interfacial region between  
15 two materials. In hybrid composites comprised of atomic layer building blocks of inorganic and  
16 organic constituents, the varying interaction between the phononic spectrum in the inorganic crys-  
17 tals and vibrionic modes in the molecular films can provide a new avenue to manipulate the energy  
18 exchange between the fundamental vibrational energy carriers across interfaces. Here, we system-  
19 atically study the heat transfer mechanisms in hybrid superlattices of atomic- and molecular-layer-  
20 grown zinc oxide and hydroquinone with varying thicknesses of the inorganic and organic layers  
21 in the superlattices. We demonstrate ballistic energy transfer of phonons in the zinc oxide that is  
22 limited by scattering at the zinc oxide/hydroquinone interface for superlattices with a single mono-  
23 layer of hydroquinone separating the thicker inorganic layers. The concomitant thermal boundary  
24 conductance across the zinc oxide interfacial region approaches the maximal thermal boundary  
25 conductance of a zinc oxide phonon flux, indicative of the contribution of long wavelength vibra-  
26 tions across the aromatic molecular monolayers in transmitting energy across the interface. This  
27 transmission of energy across the molecular interface decreases considerably as the thickness of the  
28 organic layers are increased.

29 PACS numbers: 66.70.-f, 63.22.-m, 68.35.-p, 68.37.-d

## 30 I. INTRODUCTION

31 The introduction of material interfaces in solid nanocomposites has provided the op-  
32 portunity for user-defined thermal transport in nanosystems through manipulation of the  
33 fundamental carriers of heat. The inclusion of these interfaces gives rise to both phonon-  
34 boundary scattering, effectively reducing the thermal conductivity of the solid due to clas-  
35 sical size effects,<sup>1</sup> and/or partial transmission of thermal energy across the interface driving  
36 the thermal boundary conductance.<sup>2,3</sup> To atomistically manipulate the phonon thermal con-  
37 ductivity of a nanosystem with a high density of material interfaces, an understanding of  
38 the interplay and relationship of phonon-boundary scattering and thermal boundary con-  
39 ductance across the interfaces must be understood.<sup>4</sup> Given that the structural and chemical  
40 properties of solid interfaces can strongly influence the thermal boundary conductance,<sup>5</sup>  
41 the ballistic or diffusive nature of phonon transport, along with the corresponding phonon  
42 wavelengths,<sup>6</sup> can affect how energy is scattered and/or transmitted across an interfacial  
43 region between two materials. This ballistic to diffusive crossover of phonon transport and  
44 energy transmission across an atomically thin interface is poorly understood.

45 The consideration of these ballistic and diffusive interfacial phonon energy transport pro-  
46 cesses has major implications for the development of novel nanomaterials for applications  
47 such as thermoelectric energy conversion,<sup>7-9</sup> where careful placement of interfaces has proven  
48 to be useful in efficiently lowering the phononic conductivity while still maintaining elec-  
49 tronic conductivity. As an example of a novel class of nanocomposites of recent interest,  
50 hybrid organic-inorganic nanomaterials grown by a combined alternation of atomic layer  
51 deposition (ALD) and molecular layer deposition (MLD) have exhibited enhanced electri-  
52 cal, optical, magnetic and mechanical functionalities compared to conventional organic or  
53 inorganic materials.<sup>10-13</sup> For example, using this ALD/MLD technique, inorganic/organic  
54 superlattices (SLs) have shown promise as potential thermoelectric materials.<sup>14,15</sup> However,  
55 paramount in advancing ALD/MLD hybrid structures for use in thermoelectric, or other  
56 applications, is an understanding of the phonon transport and scattering processes in these  
57 materials; referring to ALD/MLD SLs, this requires understanding phonon scattering at the  
58 ALD/MLD boundary, and its correlation with phonon transmission and resulting bound-  
59 ary conductance across the molecular interface. There have been limited previous works  
60 focusing on measurements of thermal conductivity of ALD/MLD grown materials.<sup>14,16-18</sup>

61 Given the high density of molecular interfaces in these composite systems, advances in the  
62 thermophysics of these materials rely on understanding the thermal conductance across the  
63 molecular interfaces.

64 Given the recent interest in thermal transport in organic-based nanocomposites<sup>19-23</sup> and  
65 heat transport across molecular interfaces,<sup>24-30</sup> systematically studying the thermal con-  
66 ductivity of a series of ALD/MLD-grown hybrid SLs also provides an ideal platform to  
67 advance our understanding of phonon scattering at, and heat transfer across, thin molecular  
68 interfaces. These high quality hybrid nanosystems also provide ideal materials to under-  
69 stand the heat transfer mechanisms in organic/inorganic SLs, and the interplay between  
70 phonon-boundary scattering and thermal boundary conductance across interfaces of identi-  
71 cal materials separated by a well defined molecular layer.

72 In this manuscript, we study the phonon transport mechanisms in a series of ALD/MLD  
73 grown SL thin films comprised of multiple layers of zinc oxide/hydroquinone. The series of SLs  
74 include period thicknesses varying from 0.7 nm to 13.1 nm with monolayers of hydroquinone  
75 (HQ) interspersed in-between the thicker inorganic layers of ZnO. We also study the effect  
76 of the organic layer thickness on the thermal transport across these SLs by investigating  
77 a set of samples fabricated by varying the MLD cycles while keeping the thickness of the  
78 inorganic layers constant. Additionally, we compare our results of the ZnO-based SLs to  
79 that of titanium dioxide (TiO<sub>2</sub>)-based SLs (Refs. 17 and 18), to scope the generality of our  
80 results.

81 We measure the thermal conductivity,  $\kappa$ , of the SLs providing a platform to study the  
82 role of organic interface density on phonon scattering at the inorganic/organic interface and  
83 thermal boundary conductance across the inorganic/organic/inorganic interface. We show  
84 that thermal transport in ZnO-based hybrid SLs with monolayers of HQ at an interface  
85 can be described as a boundary-scattering dominated process that is limited by the period  
86 length, thereby reducing the thermal conductance of the crystalline inorganic layer. Our  
87 model suggests that nearly the entire spectrum of phonons in the inorganic layer is limited  
88 by scattering at the inorganic/organic interface. As an alternative analysis, we determine  
89 a mean thermal boundary conductance across the inorganic/organic/inorganic interfaces.  
90 The reduction in the transmission of phonons across the ZnO/HQ/ZnO interface leads to  
91 an overall reduction in the thermal conductivity of the SLs compared to the thermal con-  
92 ductivity of a homogeneous ZnO thin film. Furthermore, as we increase the thickness of

93 the organic layers in the SLs, we observe a reduction in the phonon transmission across the  
94 inorganic/organic/inorganic interfaces in the hybrid SLs, which results in a reduction in the  
95 overall thermal conductivity of the composite.

## 96 II. EXPERIMENTAL DETAILS

97  $(\text{ZnO})_x/\text{HQ}$  (where  $x$  is the period thickness of the SL) thin films of five different pe-  
98 riodicities were grown via ALD/MLD on single crystal MgO substrates, an illustration of  
99 the structure is shown in Fig. 1a. An additional set of samples were fabricated with three  
100 different numbers of HQ layers (i.e., 3, 5 and 7 layers) in-between the ZnO layers with  $x=7.0$   
101 nm. Diethyl zinc and water were used as precursors for the ZnO layers, while hydroquinone  
102 was used for the MLD layers. The depositions were performed at  $220^\circ\text{C}$  and consisted of  
103 605 ALD/MLD cycles with an ALD:MLD cycle ratio of 99:1, 49:1, 29:1, 9:1 and 4:1. Con-  
104 trol sample of ZnO thin film with similar thickness as the hybrid SL samples were also  
105 fabricated via ALD. X-ray reflectivity (XRR) measurements with a PANalytical X'Pert Pro  
106 X-ray diffractometer were used to determine the thickness of the films ( $\sim 100$  nm) and the  
107 SL periods,  $x$ . The measured thicknesses are tabulated in Table S1 of the Supplemental  
108 Material.<sup>31</sup> A more detailed description of the film fabrication and characterization can be  
109 found in Ref. 32.

110 Characteristic XRR patterns for  $\text{ZnO}_{x=7.0\text{nm}}/5$  and 7 layers of HQ are shown in Fig. 1b.  
111 The film thickness dictates the small fringes corresponding to the interference minima and  
112 maxima of the reflected beam film-air and film-substrate interfaces, respectively.<sup>33</sup> The XRR  
113 also includes interference maxima with higher intensities that represent constructive interfer-  
114 ence from the periodic introduction of the organic layers. Figure 1c shows the characteristic  
115 grazing incidence x-ray diffraction (GIXRD) patterns for the SLs. Typically, the peaks in  
116 the XRD patterns were found to fit the typical ZnO hexagonal wurzite structure. As is clear  
117 from Fig 1c, there is almost no change in the position of the peaks for the SLs, suggesting  
118 that the crystallinity of the ZnO phase is preserved with the inclusion of the HQ layers.  
119 However, the intensity of the peaks for the SLs with higher number of organic monolayers  
120 (and ALD:MLD cycle ratios of 29:1, 9:1 and 4:1) are reduced compared to the purely ALD  
121 grown ZnO film, implying that the crystallinity is hindered to some extent for the inor-  
122 ganic constituents due to the organic monolayers. For the SL with the thinnest inorganic

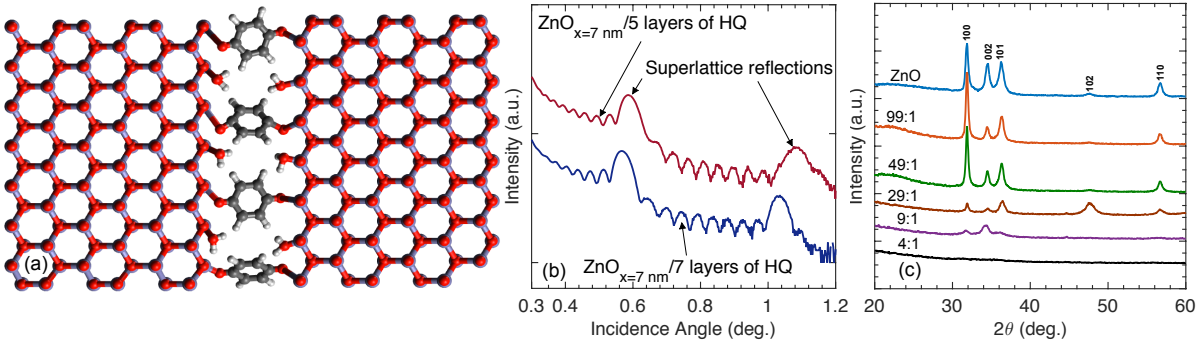


Figure 1. (a) 2D Schematic representation of the ZnO<sub>x</sub>/HQ SL. (b) Characteristic XRR patterns showing SL reflections for ZnO<sub>x</sub>/HQ with  $x=7.0$  nm with 5 and 7 layers of HQ separating the 7nm thick inorganic constituents. (c) Characteristic grazing incidence X-ray diffraction (GIXRD) patterns for the control sample and hybrid SLs with varying  $x$ . The peaks in the XRD patterns for the hybrid SLs fit to the typical hexagonal wurtzite structure of ZnO (indexed accordingly). There are no shifts in the position of the peaks for the hybrid SLs with ALD:MLD cycle ratios of 99:1, 49:1, 29:1 and 9:1, suggesting that the introduction of the organic monolayers do not affect the crystallinity of the ZnO phase.

123 constituent, the XRD pattern suggests that the inorganic constituents are amorphous.

124 We use the time domain thermoreflectance technique (TDTR) to measure the thermal  
 125 properties of the samples. The appropriate analysis procedure for these TDTR measure-  
 126 ments has been previously discussed in detail by several groups.<sup>34–36</sup> Prior to TDTR measure-  
 127 ments, we metalize the samples with a thin Al layer deposited via electron beam evaporation  
 128 at  $6 \times 10^{-6}$  Torr. In our TDTR experimental setup, laser pulses emanate from a Ti:Sapphire  
 129 oscillator with an 80 MHz repetition rate and are energetically split into pump and probe  
 130 paths. The train of ultra-short pump pulses thermally stimulate the Al metal transducer  
 131 and time delayed probe pulses measure the change in the thermoreflectance of the sample  
 132 due to the decay of the deposited thermal energy. We modulate the pump path at 8.8  
 133 MHz and monitor the ratio of the in-phase to out-of-phase signal of the probe beam from  
 134 a lock-in amplifier ( $-V_{in}/V_{out}$ ) for up to 5 ns after the initial heating event. To ensure  
 135 negligible sensitivity to in-plane transport, our pump and probe spot sizes were focused to  
 136  $1/e^2$  radii values of 30 and 9  $\mu\text{m}$ , respectively. We measure the thermoreflectance response  
 137 of each sample in a liquid nitrogen cooled cryostat from 78 to 300 K. We perform several

138 TDTR scans at different locations to ensure repeatability in our measurements. We de-  
 139 termine the thermal conductivities and thermal boundary conductances in our samples by  
 140 fitting our TDTR data to the thermal model that accounts for pulse accumulation from  
 141 the Ti:Sapphire oscillator.<sup>34-36</sup> The thickness of the Al transducer layer is measured via  
 142 picosecond acoustics.<sup>37</sup>

143 Initially, we fit the time domain thermoreflectance (TDTR) data for our ALD grown  
 144 control sample with a model that accounts for thermal diffusion in a 3 layer system by  
 145 fitting for thermal boundary conductances across the Al/ZnO and ZnO/Al<sub>2</sub>O<sub>3</sub> interfaces.  
 146 All other parameters in our thermal model such as the thermal conductivities and heat  
 147 capacities of the constituent layers are taken from literature;<sup>38-41</sup> note, due to small thermal  
 148 resistance of pure ZnO, we are negligibly sensitive to the thermal conductivity of the ZnO  
 149 thin film and our TDTR data on these control samples are dominated by the thermal  
 150 boundary conductances ( $h_K$ ) at the Al/ZnO and ZnO/Al<sub>2</sub>O<sub>3</sub> interfaces, as shown in Fig. 2a  
 151 and discussed in detail below.

152 To evaluate the thermophysical properties of interest in our control samples, namely the  
 153 thermal boundary conductances across the Al/ZnO and ZnO/Al<sub>2</sub>O<sub>3</sub> interfaces, we must  
 154 determine the appropriate range of pump-probe delay times to fit the thermal model to the  
 155 experimental data, in which the thermal model is extremely sensitive to changes in  $h_K$ .<sup>36,42</sup>  
 156 To determine these interface resistances, we use a combination of the in-phase response and  
 157 the ratio of the in-phase to out-of-phase responses over various pump-probe time delays,  
 158 due to relative sensitivities to the thermophysical properties of interest in this system. The  
 159 sensitivity of the in-phase signal to various thermal properties is defined by,

$$S_a = \frac{\partial \ln(-V_{\text{in}})}{\partial \ln(a)} \quad (1)$$

160 where  $a$  is the thermophysical parameter of interest and  $V_{\text{in}}$  is directly proportional to the  
 161 response of the thermoreflectance signal recorded by the lock-in amplifier. Figure 2a shows  
 162 the sensitivities of  $V_{\text{in}}$  to the thermophysical properties of interest in our ZnO control sample  
 163 at 300 K. The sensitivity to  $h_K$  for the Al/ZnO interface is relatively large and very dynamic  
 164 for the first nanosecond time delay at both 78 and 300 K. In this time frame, the sensitivities  
 165 of the other parameters are minimal and therefore will not affect the thermal response of the  
 166 control sample. Therefore, we fit the in-phase signal with the thermal model by iterating  
 167 the  $h_K$  for the Al/ZnO interface and all the other parameters are held constant for 1 ns



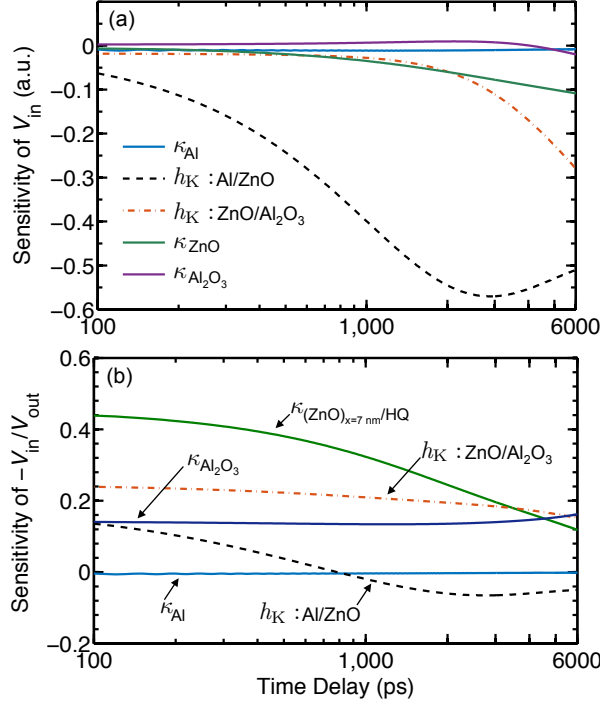


Figure 2. (a) Sensitivities of the (a) in-phase signal (for a purely ALD grown ZnO thin film) and (b) ratio of the in-phase and out-of-phase signals (for the  $(ZnO)_{x=7nm}/HQ$  film) to the thermal boundary conductances at Al/ZnO and ZnO/Al<sub>2</sub>O<sub>3</sub> interfaces and thermal conductivities of Al, ZnO and Al<sub>2</sub>O<sub>3</sub>.

168 time delay. We note that since fitting the in-phase response of the TDTR signal requires  
 169 scaling our model to the data at a fixed delay time (which we choose as 100 ps), we become  
 170 completely insensitive to thermophysical properties that have flat sensitivities in the time  
 171 domain, further enhancing our accuracy in determining  $h_K$  over our specified time delay.  
 172 Similarly, we determine the  $h_K$  for the ZnO/Al<sub>2</sub>O<sub>3</sub> interface by fitting the in-phase signal in  
 173 the range of 2-5 ns while using the  $h_K$  for the Al/ZnO interface determined from the first  
 174 1 ns time delay fit. We discuss this fitting approach in more detail in the Supplemental  
 175 Material.

176 The measured thermal boundary conductances from the control sample are used as input  
 177 parameters for thermal conductivity analyses of the superlattice samples ( $(ZnO)_x/HQ$ ). We  
 178 fit the ratio of the in-phase and out-of-phase signals ( $-V_{in}/V_{out}$ ) to the 3 layer thermal  
 179 model to determine the thermal conductivity of the superlattice films. For these fits, we use

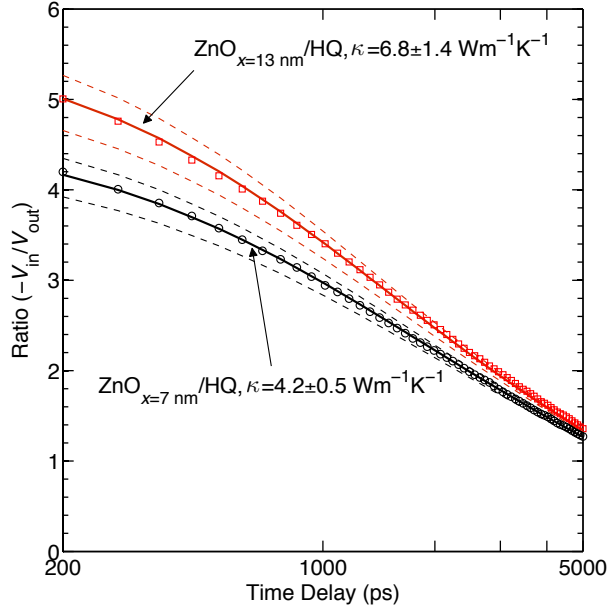


Figure 3. Sample data and best-fit curves for the  $(\text{ZnO})_{x=7.0 \text{ nm}}/\text{HQ}$  (red squares) and  $(\text{ZnO})_{x=13.1 \text{ nm}}/\text{HQ}$  (black circles) along with uncertainties (dotted lines) at room temperature.

180 the thermal boundary conductances determined from our in-phase analyses, leaving the only  
 181 unknown parameter in these measurements as the thermal conductivity of the  $(\text{ZnO})_x/\text{HQ}$   
 182 films. Figure 2b shows the sensitivity of the ratio to the various parameters in our 3-  
 183 layer model for the  $(\text{ZnO})_{x=7\text{nm}}/\text{HQ}$  film. An error of 15% in  $h_K$  for the Al/ZnO interface  
 184 propagates to an error of  $\sim 1.5\%$  and  $\sim 0.8\%$  on the measured thermal conductivities of  
 185 the  $(\text{ZnO})_{x=13.1 \text{ nm}}/\text{HQ}$  and  $(\text{ZnO})_{x=7.0 \text{ nm}}/\text{HQ}$  samples at room temperature, respectively.  
 186 However, an error of 15% in  $h_K$  for the ZnO/ $\text{Al}_2\text{O}_3$  interface causes an error of  $\sim 13\%$  and  
 187  $\sim 7\%$  in the measured conductivities for  $(\text{ZnO})_{x=13.1 \text{ nm}}/\text{HQ}$  and  $(\text{ZnO})_{x=7.0 \text{ nm}}/\text{HQ}$  samples  
 188 at room temperature, respectively. This is a major source of uncertainty reported for our  
 189 measurements. The fits to the TDTR data along with the uncertainties (dashed lines) for  
 190 the samples  $(\text{ZnO})_{x=7.0 \text{ nm}}/\text{HQ}$  and  $(\text{ZnO})_{x=13.1 \text{ nm}}/\text{HQ}$  at 300 K are shown in Fig. 3.

### 191 III. RESULTS AND DISCUSSIONS

192 Figure 4 shows the measured thermal conductivities for the  $(\text{ZnO})_x/\text{HQ}$  SLs with varying  
 193  $x$  at different sample temperatures. The thermal conductivities of these SLs demonstrate

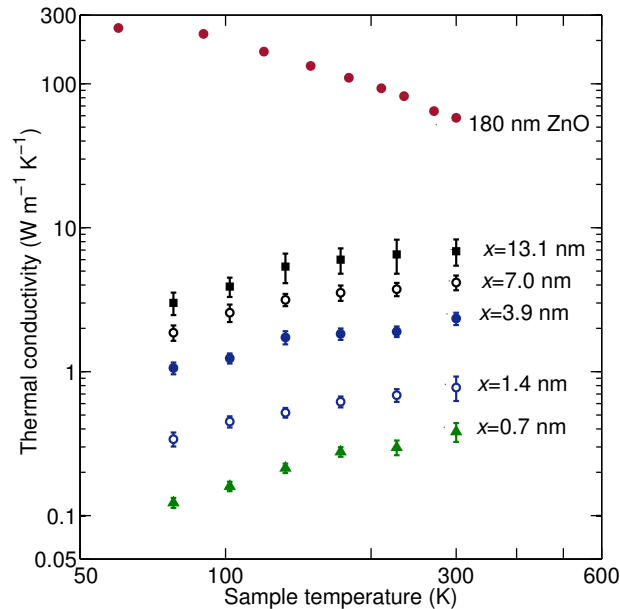


Figure 4. Measured thermal conductivities as a function of temperature for  $(\text{ZnO})_x/\text{HQ}$  SLs with varying  $x$ . The error bars include uncertainties due to repeatability, Al thickness measurement and uncertainties in the parameters used in the thermal model. Also plotted are the thermal conductivities for a 180 nm ALD-grown homogenous ZnO film taken from Ref. 39.

194 more than a ten-fold decrease compared to the results for an ALD-grown homogeneous ZnO  
 195 thin film<sup>39</sup> as shown in Fig. 4. The inclusion of higher interface densities and the reduction  
 196 in the inorganic layer thickness results in the reduction of the thermal conductivities of these  
 197 hybrid SLs.

198 To describe the results in Fig. 4, we consider the thermal transport in these hybrid  
 199 samples being described by a phonon flux in the inorganic material that is limited only by  
 200 phonon/boundary scattering at the inorganic/organic interface. In other words, we assume  
 201 that the overall thermal conductivities of the SL films are minimally affected by scattering  
 202 mechanisms in the bulk of the inorganic constituent (such as phonon-defect or phonon-  
 203 phonon scattering in the individual layers). Therefore, the thermal transport is limited by  
 204 the combination of the phonon flux,  $q$ , in the inorganic layers and the thickness,  $x$ , of the  
 205 layers (i.e.,  $x$  = period thickness of the SLs). The phonon flux in the inorganic layer can be

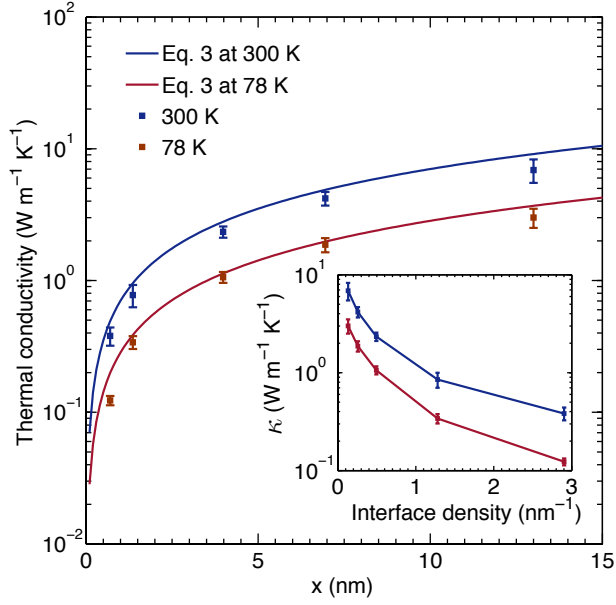


Figure 5. Thermal conductivity as a function of the inorganic layer thickness for SLs with single HQ layers at 78 K and 300 K. Along with that, the predicted thermal conductivities as a function of SL period thickness calculated from Eq. 2 at 78 K and 300 K are also shown. The effective thermal conductivity model assuming only phonon-boundary scattering at the HQ-layer interface described in Eq. 3 provides reasonable agreement with the measured thermal conductivities for these SLs. (inset) The thermal conductivity for these hybrid SLs is inversely proportional to the ZnO/HQ/ZnO interface density.

206 approximated by,<sup>43</sup>

$$q = \frac{1}{8\pi^2} \sum_j \int_{k_1} \hbar \omega k^2 v_j f dk \quad (2)$$

207 where,  $j$  is the polarization,  $\omega$  is the phonon frequency,  $\hbar$  is Planck's constant,  $f$  is the  
 208 Bose-Einstein distribution and  $v$  is the group velocity. Equation 1 assumes an isotropic,  
 209 spherical Brillouin zone to predict the heat flux in the inorganic ZnO layers. We note that  
 210 this assumption correctly predicts the volumetric heat capacity of ZnO (further details of  
 211 the assumptions and our calculations are provided in the Supplemental Material). With the  
 212 flux,  $q$ , determined from the phonon dispersion, the effective thermal conductivity of the

213 SLs that is dictated by the period thickness  $x$ , is given by,

$$\kappa_{\text{effective}} = \frac{1}{3} \int C_k v_k dk \ x = \frac{\partial q}{\partial T} x \quad (3)$$

214 where  $T$  is temperature and  $C_k$  is the spectral phonon heat capacity. Equation 3 assumes  
215 that phonon transport in the inorganic layer is ballistic and that the phonons scatter only  
216 at boundaries that restore local thermodynamic equilibrium. As such, our discussion and  
217 analyses assume that the interfacial organic boundaries are considered to be reflectionless  
218 and black, and the phonon flux is assumed to thermalize at these boundaries. Calculations  
219 of Eq. 3 for ZnO at two temperatures as a function of  $x$  are shown in Fig. 5. For these  
220 calculations, we use all 12 branches of the bulk phonon dispersion relation for ZnO in the  
221  $\Gamma \rightarrow M$  direction, as calculated in Ref. 44 via *ab initio* methods. The measured thermal  
222 conductivities at 78 K and 300 K for the SLs show good agreement with our calculations  
223 of Eq. 3, supporting our assertion that size effects in the inorganic layers of the hybrid SLs  
224 limit thermal transport. This analysis assumes that the entire spectrum of phonon mean free  
225 paths in the ZnO layer is limited by scattering at the inorganic/organic/inorganic interface.

226 The drastic reduction in the thermal conductivity values decreasing period in the SLs is  
227 clearly seen by the inverse relationship of  $\kappa$  with ZnO/HQ/ZnO interface density as shown  
228 in the inset of Fig. 5. To scope the generality of these results to hybrid SLs, we compare the  
229 measured thermal conductivity of  $3.1 \pm 0.2 \text{ W m}^{-1} \text{ K}^{-1}$  for a  $(\text{TiO}_2)_x/\text{HQ}$  SL with  $x=15.5$   
230 nm at room temperature to the thermal conductivity measurement for a homogeneous  $\text{TiO}_2$   
231 thin film ( $5.2 \pm 0.3 \text{ W m}^{-1} \text{ K}^{-1}$ ).<sup>17,18</sup> The reduction in thermal conductivity for the  $\text{TiO}_2$ -  
232 based SL is in line with the results reported for the  $(\text{ZnO})_x/\text{HQ}$  SLs. This reduction in  
233 the thermal conductivity due to the periodic monolayers is consistent with the decrease in  
234 thermal conductivity with increased interface density in inorganic SLs.<sup>45,46</sup>

235 As pointed out in purely inorganic SLs, the monotonic decrease in thermal conductivity  
236 due to increased interface density (and linearly increasing thermal resistance with increasing  
237 interface density) is due to incoherent scattering, where the phonons behave as particles and  
238 lose their phase information by scattering at the internal boundaries.<sup>45,46</sup> Ravichandran  
239 *et al.*<sup>45</sup> have shown that by increasing the interface density (decreasing period thicknesses)  
240 beyond the incoherent regime, the phonon dispersion in inorganic SLs can be altered by  
241 mini-band formation, which effectively preserves the coherent nature of phonon transport  
242 in these SLs. An alternative wave nature of phonon transport in inorganic SLs has also

243 been demonstrated by Luckyanova *et al.*,<sup>47</sup> where they varied the total thickness of the  
244 inorganic SL films while keeping the SL period thicknesses constant and showed an increase  
245 in the thermal conductivity. Our results for the hybrid SLs are consistent with the particle  
246 nature of phonon transport (or the incoherent scattering regime) as demonstrated by the  
247 monotonically decreasing thermal conductivity with increasing interface densities (see inset  
248 of Fig. 5).

249 The appreciable agreement between our measured values for a wide range of inorganic  
250 layer thicknesses and that predicted by the model in Eq. 3 (as shown in Fig. 5) suggests that  
251 the phonon flux in the inorganic layer is mostly ballistic and the phonon mean free path is  
252 limited by the ZnO layer thicknesses. However, for thicker inorganic layers, where phonon-  
253 phonon scattering in the bulk of the inorganic layer creates a temperature gradient along  
254 the layer, the validity of Eq. 3 in describing thermal transport in these SLs is questionable.  
255 In fact, this is exemplified by the disagreement between the prediction of Eq. 3 for  $x = 13.1$   
256 nm and the experimentally measured  $\kappa$  for  $(\text{ZnO})_{x=13.1\text{nm}}/\text{HQ}$ . Therefore, by describing the  
257 thermal transport by Eq. 3, we have considered the thermal conductivities of these hybrid  
258 SLs to be driven by a ballistic phonon flux limited by scattering at the inorganic/organic  
259 interface, which clearly breaks down as the ZnO thickness increases. Therefore, to study the  
260 validity and range of applicability of this hypothesis, we consider an alternative analysis of  
261 our results in Figs. 4 and 5 by considering the reduction in thermal conductivity to be driven  
262 by a thermal boundary conductance across the inorganic/organic/inorganic interface. This  
263 approach will give quantitative insight into the role of phonon transmission across the inor-  
264 ganic/organic/inorganic interface on our measured thermal conductivities. Note, as we are  
265 not able to separate the individual resistances due to scattering at the ZnO/HQ boundaries  
266 and the internal scattering in the HQ layer, we couple these scattering mechanisms into a  
267 lumped resistance in our discussions and analysis presented below.

268 In the typical semi-classical picture of thermal boundary conductance across solid inter-  
269 faces (i.e., the acoustic or diffuse mismatch models<sup>2,48,49</sup>), a mismatch in acoustic properties  
270 or vibrational density of states, limits the interfacial phonon transmission, and therefore  
271 restricts the phonon flux that transmits across the organic-based interfaces. The acoustic  
272 mismatch model (AMM) considers phonons as plane waves and the lattice as a continuum  
273 solid and assumes specular reflection and transmission of phonon energy at the interface,  
274 whereas the diffuse mismatch model (DMM) disregards this complete specularly at the

275 interface. These models could potentially offer complementary, yet alternative insight into  
 276 the mechanisms driving the large reduction in the measured thermal conductivity of these  
 277 hybrid SLs, and elucidate the role of the organic monolayers and their intrinsic vibrational  
 278 properties on phonon transport. We model the thermal boundary conductance ( $h_K$ ) through  
 279 the organic interface, which is described by the temperature derivative of the phonon flux  
 280 (as described in Eq. 2) with the inclusion of a transmission coefficient ( $\zeta_{1\rightarrow 2}$ ) from side 1 to 2  
 281 (from inorganic, through the organic monolayer, and emitted into the next inorganic layer).  
 282 The thermal boundary conductance is defined based on the temperature of the incident  
 283 and emitted phonons, and therefore it predicts a finite interfacial conductance (as opposed  
 284 to an infinite conductance or zero thermal boundary resistance) for an imaginary interface  
 285 comprising of the same material.<sup>50</sup> This conductance occurs when  $\zeta_{1\rightarrow 2}=1$  and all available  
 286 phonon modes are transmitted from side 1 to 2 of the imaginary interface in the crystal. We  
 287 note that by this definition, the maximum possible thermal boundary conductance for an  
 288 imaginary interface is solely limited by the phonon flux that impinges upon the interface.  
 289 Alternatively, assuming an interface between two materials that causes diffusive scattering,  
 290 this maximum limit is described by a transmission of  $\zeta=0.5$ .

291 To consider the possibility of the thermal boundary conductance across the inor-  
 292 ganic/organic/inorganic interface-limiting the thermal transport across the SLs, we model  
 293  $h_K$  across the ZnO/HQ/ZnO interface assuming maximal phonon transmission. This as-  
 294 sumption implies that the phonon transmission from the ZnO across the HQ is unimpeded  
 295 by any properties of the HQ; that is, we assume  $\zeta_{1\rightarrow 2}=1$ . For these calculations, we make the  
 296 same assumptions for ZnO density of states and phonon velocities as in Eq. 2. Calculation  
 297 of this maximal conductance at room temperature for a ZnO phonon flux is shown in Fig. 6a  
 298 (dashed line). In most real nanosystems, due to both a mismatch of vibrational density  
 299 of states and imperfections around the interfacial regions, the transmission coefficient is  
 300 not unity (for a review of thermal boundary conductance dictated by various interfacial  
 301 conditions, readers are referred to Ref. 5). For this reason, the measured values of  $h_K$  in  
 302 the literature have never exceeded this maximum thermal boundary conductance for any  
 303 interface.

304 From the measured thermal conductivities in our hybrid SLs, we derive the mean thermal  
 305 boundary conductance across the individual ZnO/HQ/ZnO interfaces with a series resistor  
 306 model, which assumes that phonons can only scatter at the ZnO/HQ/ZnO interfaces (con-

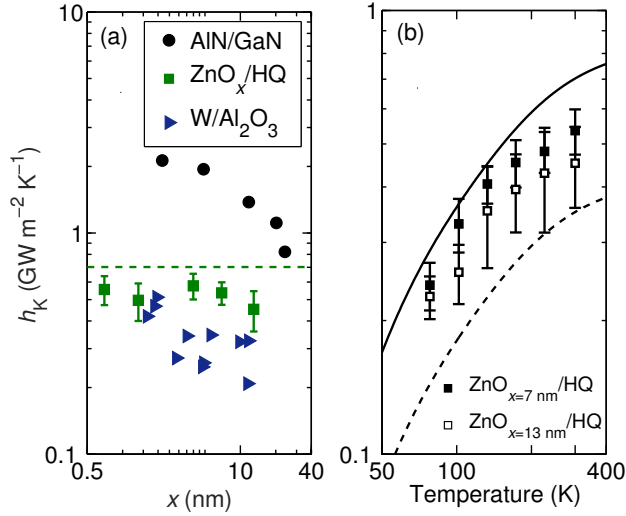


Figure 6. (a) The mean thermal boundary conductances of interfaces in ZnO<sub>x</sub>/HQ SLs derived from thermal conductivity measurements shown in Fig. 4. Also plotted are the mean conductances of interfaces in W/Al<sub>2</sub>O<sub>3</sub> SLs<sup>51</sup> and AlN/GaN SLs<sup>52</sup> for comparison (b) The mean thermal boundary conductances derived for  $x=7.0$  nm and 13.1 nm as a function of temperature for the ZnO based SLs. The calculations of maximum conductance in ZnO with phonon transmission coefficient equal to unity are also shown. Also included for comparison is the calculation of the DMM for a ZnO/ZnO interface (i.e., 50% transmission of the ZnO phonon flux).

307 sistent with our previous analysis where we assume that the phonon flux is only scattered  
 308 at the ZnO/HQ boundaries). We calculate the mean conductance across the HQ layers as  
 309  $h_K = 1/R_K = (\kappa_{\text{ZnO}_x/\text{HQ}} n)/d$ , where  $n$  is the number of inorganic/organic/inorganic in-  
 310 terfaces and  $d$  is the total thickness of the hybrid films. To reiterate, this formulation of  
 311  $1/R_K$  implies that the resistance due to the individual ZnO/HQ interfaces and the intrinsic  
 312 resistance of the organic molecules comprising the interface are lumped as a single resistor.

313 Figure 6a shows the mean thermal conductance for ZnO/HQ/ZnO interfaces as a func-  
 314 tion of the inorganic layer thickness (hollow squares). Two aspects of the results for the  
 315 conductance calculations shown in Fig. 6a are worth noting. First, the values of the mean  
 316 conductances for these SLs among the various samples are agreeable within the uncertain-  
 317 ties, regardless of the ZnO/HQ/ZnO interface density. This suggests that the series resis-  
 318 tor model used to derive these conductances is applicable for our hybrid SLs with single



319 HQ layers, and our previous assumption and discussion regarding fully thermalizing (i.e.,  
320 black) inorganic/organic boundaries is supported. Along with the results for the hybrid SLs,  
321 we also plot the mean conductances derived from thermal conductivity measurements for  
322 W/Al<sub>2</sub>O<sub>3</sub>,<sup>51</sup> and AlN/GaN<sup>52</sup> SLs. Contrary to our hybrid SLs, the mean conductances in  
323 these inorganic based SLs increase with decreasing period thicknesses. In Ref. 52, this in-  
324 crease in  $h_K$  for the AlN/GaN SLs was attributed to phonons with long wavelengths carrying  
325 the majority of heat.

326 The second aspect worth noting is that the mean conductances derived are close to the  
327 maximum conductance with  $\zeta = 1$ . We demonstrate this consistency over a wide range  
328 of temperatures, shown in Fig. 6b, which plots  $h_K$  calculated for ZnO/HQ/ZnO interface  
329 as a function of temperature for the two SLs with  $x=13.1$  nm and 7.0 nm. The appre-  
330 ciable agreement between these values and the conductance in ZnO is consistent with the  
331 analysis in Fig. 5 (treating all phonon mean free paths being limited by scattering at the  
332 ZnO/HQ/ZnO interface), as mentioned above. This agreement also suggests that a large  
333 portion of the phonon modes in the ZnO transmits ballistically across the ZnO/HQ/ZnO in-  
334 terface, implying relatively minor intrinsic thermal resistance in the molecular layer. While  
335 the relatively minor disagreement between the maximal conductance (Fig. 6b, solid line) and  
336 the data could imply some level of phonon-vibron interactions in the HQ layer, more rig-  
337 orous computational models are necessary to draw quantitative conclusions regarding these  
338 diffusive scattering processes in the molecule.

339 In order to quantify the contribution of the vibrational properties of the organic layer on  
340 phonon transmission across the ZnO/HQ/ZnO interfacial region, we calculate the average  
341 phonon transmissions from the results in Fig. 6b (comparing the maximal conductance model  
342 to the data) and find interfacial transmissions of  $\sim 76\%$  for the (ZnO)<sub>7.0 nm</sub>/HQ sample and  
343  $\sim 65\%$  for the (ZnO)<sub>13.1 nm</sub>/HQ sample at room temperature. This deviation from “perfect”  
344 transmission of phonons could be due to the fact that heat flux carried by phonons with  
345 wavelengths longer than the organic molecular chain lengths are unaffected by the organic  
346 layer, whereas phonons with wavelengths on the order of and smaller than the molecular  
347 lengths are scattered due to the vibrational properties of the molecules (as discussed in more  
348 detail in the Supplemental Material). We note that 75-91% of the phonon flux in ZnO is  
349 carried by phonons with wavelengths longer than the average thickness of the HQ layer (Sup-  
350 plemental Material), supporting this hypothesis. We note that this hypothesis is consistent

351 with previous works suggesting that at interfaces, the transmission of phonon wavelengths  
352 greater than the characteristic length scales of nanoscale structures and asperities at solid  
353 interfaces are not affected by these non-idealities.<sup>5,6,52-55</sup> More rigorous computational sim-  
354 ulations are necessary to study this hypothesis in more detail, which includes a greater  
355 understanding of diffusive vibrational scattering in single-molecule thick films as previously  
356 mentioned.

357 One of the factors driving the high phonon transmission values across ZnO/HQ/ZnO  
358 interfaces could be due to the high quality interfaces within the SLs and the precise control  
359 over the thicknesses of the inorganic layers achieved via the layer-by-layer deposition of the  
360 ALD/MLD technique.<sup>17,56</sup> At the inorganic/organic interfaces, it has been shown through  
361 first principles study that the HQ molecules are most probably attached to every other sur-  
362 face Zn site (50 % surface coverage).<sup>57</sup> This implies that we can not rule out the possibility of  
363 ZnO growth at the lateral interstitial positions, which could affect the phonon energy trans-  
364 mission across these inorganic/organic/inorganic interfaces; in principle this could happen if  
365 the physical size of the HQ would prevent its reaction with all the Diethyl zinc terminated  
366 surface sites. However, the systematically lower densities (predicted from XRR measure-  
367 ments, and reported in the Supplemental Materials) with increasing number of MLD cycles,  
368 suggest that the presence of interstitial ZnO within the organic layers is unlikely.

369 The implication of large thermal transmission across the single HQ layer assumes that  
370 there is no mismatch of acoustic impedance or vibrational spectra encountered by the im-  
371 pinging ZnO flux on the HQ monolayer. Although this would be true for a pure ZnO/ZnO  
372 interface in which phonons are specularly scattered, this clearly would not be the case if  
373 considering phonon thermal conductance limited by transmission across the ZnO/HQ/ZnO  
374 interface due to properties of the HQ. To exemplify this more quantitatively, we performed  
375 molecular dynamics simulations on a plane of HQ molecules to obtain the power spectral  
376 density. The power spectral density is compared to the  $D(\omega)$  spectrum for bulk ZnO cal-  
377 culated from the phonon dispersion,<sup>44</sup> and as expected, the relatively discrete modes in the  
378 phonon frequencies calculated for the HQ layer do not completely overlap the  $D(\omega)$  for ZnO  
379 (Fig. S6 in Supplemental Material). Note, we do not attempt to separate the scattering  
380 at the ZnO/HQ boundary from the internal scattering within the organic monolayers from  
381 our MD simulations, which is beyond the scope of this study. However, from our predicted  
382 phonon density of states for a confined HQ layer mimicking a 50 % surface coverage, we can

383 infer that under the typical DMM picture of phonon transmission from the ZnO across the  
384 HQ and into the next ZnO layer, a HQ-limited transmission seems implausible.

385 To scope the generality of the discussions presented above, we derive the conductance  
386 across the  $\text{TiO}_2/\text{HQ}/\text{TiO}_2$  from the thermal conductivity measurement for the  $\text{TiO}_2$ -based  
387 SL at room temperature<sup>17</sup> and compare the value to the result for a control sample with-  
388 out the HQ layers ( $\text{Al}/\text{TiO}_2/\text{MgO}$ ). We determine  $h_K = 430 \pm 78 \text{ MW m}^{-2} \text{ K}^{-1}$  for  
389  $\text{TiO}_2/\text{HQ}/\text{TiO}_2$  interface, lower than that of the ZnO-based SLs at room temperature.  
390 From this, we determine the phonon transmission across the  $\text{TiO}_2/\text{HQ}/\text{TiO}_2$  interface to be  
391  $\sim 41\%$ . Further calculations of the spectral heat flux as a function of the wave-vector for  
392  $\text{TiO}_2$  (Supplemental Material) demonstrates that the percent heat flux carried by phonons  
393 with wavelengths shorter than  $\sim 6\text{-}7 \text{ \AA}$  in  $\text{TiO}_2$  is  $\sim 53\text{-}62\%$ , in reasonable agreement with  
394 the  $\sim 41\%$  transmission determined for the  $\text{TiO}_2$ -based sample.

395 In order to investigate the role of molecular vibrations on the phonon scattering mecha-  
396 nisms, we measured the thermal conductivities of SLs with 3, 5 and 7 layers of HQ molecules  
397 interspersed between  $x=7.0 \text{ nm}$  thick ZnO layers at room temperature (see top panel of Fig. 7  
398 for depictions of unit cells<sup>57</sup>). As shown in Fig. 7a, increasing the number of MLD cycles  
399 for the SLs decreases the thermal conductivity monotonically. Note, the prediction of Eq. 3  
400 for  $x = 7 \text{ nm}$  does not agree with the measurements for thicker HQ layers, which we ascribe  
401 to ZnO phonons scattering in the organic layers due to the vibrational properties of the  
402 thicker HQ layers. To further quantify the role of the vibrational resistance on these com-  
403 posite structures, we plot the mean thermal boundary resistance across the ZnO/HQ/ZnO  
404 interface as a function of number of molecular layers in Fig. 7b as calculated from the series  
405 resistor model. The linear trend in resistance as the HQ layer is increased from 3 to 7 layers  
406 suggests that the internal diffusive scattering in the organic layer plays a significant role in  
407 impeding thermal transport for SLs with greater than or equal to 3 layers of HQ in-between  
408 the inorganic layers. We note that from GIXRD measurements, we do not observe a sig-  
409 nificant reduction in the crystallinity of the inorganic constituents due to inclusion of the  
410 thicker HQ layers, implying that the reduction in thermal conductivities of these structures  
411 with 3 to 7 HQ layers is mainly due to scattering at the thicker HQ layers.

412 We gain quantitative support for this result by calculating the average phonon trans-  
413 mission from the ZnO across the HQ layer using the approach discussed previously (trans-  
414 missions shown in Fig. 7b). Increasing the MLD cycles from a monolayer to 3 HQ layers

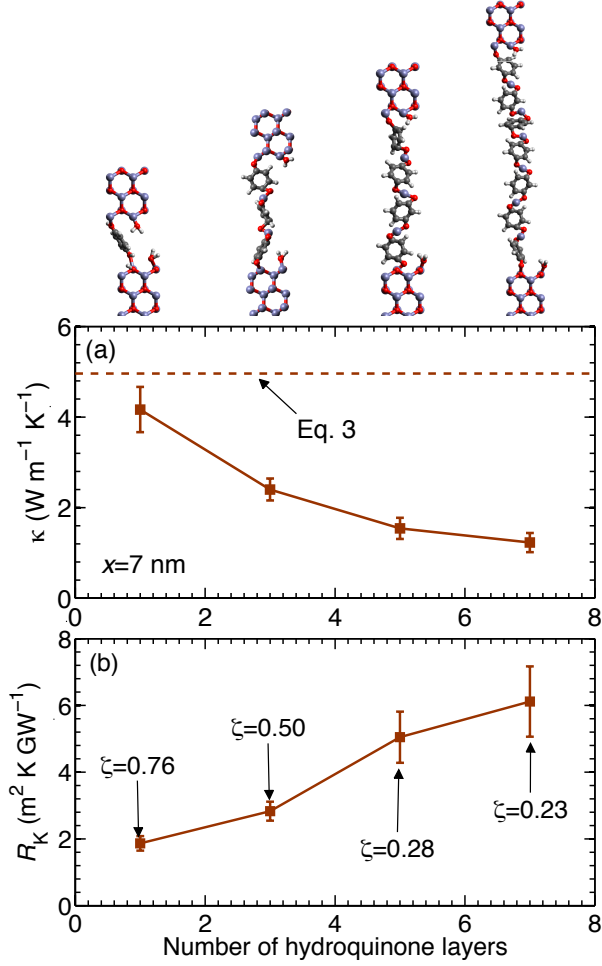


Figure 7. Top panel depicts unit cells with increasing number of hydroquinone molecules. (a) Thermal conductivity measurements at room temperature as a function of the number of MLD cycles performed. Calculation of Eq. 2 for the inorganic layer thickness is also shown for comparison. The measured thermal conductivity for the SLs deviate from the prediction of Eq. 3 as the HQ layer thicknesses increase. (b) Effective resistances of inorganic/organic/inorganic interfaces with varying number of hydroquinone layers derived from the thermal conductivities shown in (a).

415 drastically reduces the transmission from 76% to 53%. Upon further increase in the number  
 416 of HQ layers to 5 and 7, the transmissions reduce to 28% and 23%, respectively. Previous  
 417 studies on the length dependent vibrational transport in molecular chains have mostly fo-  
 418 cused on self assembled monolayers of aliphatic alkane chains.<sup>27,58-60</sup> Most of these studies  
 419 have concluded that the conductance across molecular chains is insensitive to the length of  
 420 the hydrocarbon chains, particularly in Ref. 60, it is shown that the conductance is constant

421 for chain lengths  $>20$  carbon atoms. However, for shorter chain lengths, theoretical calcula-  
422 tions by Segal *et. al.*<sup>60</sup> and experimental data by Meier *et. al.*<sup>59</sup> suggest that conductance is  
423 maximum for a chain length of up to 4 carbon atoms and decreases with increasing number  
424 of carbon atoms thereafter to a certain chain length. From our results, the drastic reduction  
425 in phonon transmission coefficients with thicker HQ layers compared to that of the SLs with  
426 a monolayer of HQ molecule could be due to the diffusive nature of vibrational transport  
427 in the longer chain molecules. However, as pointed out previously, we cannot comprehen-  
428 sively separate the resistances due to inorganic/organic interface scattering and the internal  
429 scattering in the molecular layers. Therefore, we do not attempt to separate the intrinsic  
430 thermal conductivity of the individual organic layers from the overall thermal conductivity  
431 of the hybrid films.

#### 432 IV. CONCLUSIONS

433 We conclude that the heat transfer mechanisms in hybrid SLs with single molecular layers  
434 are driven by phonon-boundary scattering, where the entire spectrum of phonon mean free  
435 paths in the inorganic layer is limited by scattering at the inorganic/organic interface. The  
436 resulting thermal conductivities of these hybrid nanostructures are mainly limited by the  
437 ZnO phonon flux and period spacing of the inorganic layers. Our analysis suggests that the  
438 phonon flux in the inorganic layer, which scatters at the inorganic/organic interface, limits  
439 the thermal conductivity of these nanostructures. The mean conductances derived from  
440 the thermal conductivity measurements also suggest that scattering at the molecular layer  
441 interfaces accounts for the majority of the reduction in the thermal conductivity of hybrid  
442 SLs with single organic layers. By considering this as a thermal boundary conductance lim-  
443 ited processes, we hypothesize that phonons with wavelengths greater than the organic layer  
444 thickness are transmitted across the organic layers after scattering at the inorganic/organic  
445 interface; these phonon wavelengths make up  $>75\%$  of the phonon flux in the ZnO, which  
446 offers a concomitant picture of the heat transfer processes in inorganic/organic hybrid com-  
447 posites. By increasing the thickness of the MLD-grown layer, we observe a significant re-  
448 duction in the phonon transmission across the thicker molecular layers as compared to the  
449 thermal conductance across the single organic layers. The linear trend in thermal resistance  
450 with number of molecular layers suggests a diffusive scattering process in the MLD-grown or-

451 ganic layer, which offers a robust opportunity for more focused theoretical or computational  
452 studies to pinpoint the size effects in vibronic scattering in aromatic molecules.

### 453 ACKNOWLEDGEMENT

454 PEH appreciates support from the United States Army Research Office (W911NF-13-1-  
455 0378). MK appreciates support from the Aalto Energy Efficiency Research Programme and  
456 the European Research Council under the European Union’s Seventh Framework Programme  
457 (FP/2007-2013)/ERC Advanced Grant Agreement (No. 339478).

---

458 \* phopkins@virginia.edu

459 <sup>1</sup> G. Chen, *Nanoscale Energy Transport and Conversion: A Parallel Treatment of Electrons,*  
460 *Molecules, Phonons, and Photons (MIT-Pappalardo Series in Mechanical Engineering)* (Oxford  
461 University Press, USA, 2005).

462 <sup>2</sup> E. T. Swartz and R. O. Pohl, *Reviews of Modern Physics* **61**, 605 (1989).

463 <sup>3</sup> P. L. Kapitza, *Zhurnal eksperimentalnoi i teoreticheskoi fiziki* **11**, 1 (1941).

464 <sup>4</sup> It is important to note that the reduction in the thermal conductivity of a material due to phonon  
465 boundary scattering may not be entirely correlated to the intrinsic thermal boundary conduc-  
466 tance between two solids, and is influenced by ballistic transport and phonon mean free paths  
467 incident upon the interface, as has been shown both computationally<sup>61</sup> and experimentally<sup>52</sup>.

468 <sup>5</sup> P. E. Hopkins, *ISRN Mechanical Engineering* **2013**, 682586 (2013).

469 <sup>6</sup> R. Cheaito, J. T. Gaskins, M. E. Caplan, B. F. Donovan, B. M. Foley, A. Giri, J. C. Duda, C. J.  
470 Szejewski, C. Constantin, H. J. Brown-Shaklee, J. F. Ihlefeld, and P. E. Hopkins, *Phys. Rev.*  
471 *B* **91**, 035432 (2015).

472 <sup>7</sup> N. Mingo, D. Hauser, N. P. Kobayashi, M. Plissonnier, and A. Shakouri, *Nano Letters* **9**, 711  
473 (2009).

474 <sup>8</sup> S. J. Poon and K. Limtragool, *Journal of Applied Physics* **110**, 114306 (2011).

475 <sup>9</sup> J. Tang, H.-T. Wang, D. H. Lee, M. Fardy, Z. Huo, T. P. Russell, and P. Yang, *Nano Letters*  
476 **10**, 4279 (2010).

477 <sup>10</sup> Y. Chujo, *Current Opinion in Solid State and Materials Science* **1**, 806 (1996).

- 478 <sup>11</sup> P. Judeinstein and C. Sanchez, *J. Mater. Chem.* **6**, 511 (1996).
- 479 <sup>12</sup> B. Yoon, B. H. Lee, and S. M. George, *The Journal of Physical Chemistry C* **116**, 24784 (2012).
- 480 <sup>13</sup> K.-H. Yoon, K.-S. Han, and M.-M. Sung, *Nanoscale Research Letters* **7**, 71 (2012).
- 481 <sup>14</sup> T. Tynell, A. Giri, J. Gaskins, P. E. Hopkins, P. Mele, K. Miyazaki, and M. Karppinen, *J.*  
482 *Mater. Chem. A* **2**, 12150 (2014).
- 483 <sup>15</sup> T. Tynell, I. Terasaki, H. Yamauchi, and M. Karppinen, *J. Mater. Chem. A* **1**, 13619 (2013).
- 484 <sup>16</sup> J. Liu, B. Yoon, E. Kuhlmann, M. Tian, J. Zhu, S. M. George, Y.-C. Lee, and R. Yang, *Nano*  
485 *Letters* **13**, 5594 (2013).
- 486 <sup>17</sup> J.-P. Niemelä, A. Giri, P. E. Hopkins, and M. Karppinen, *J. Mater. Chem. A* **3**, 11527 (2015).
- 487 <sup>18</sup> A. Giri, J.-P. Niemelä, C. J. Szwejkowski, M. Karppinen, and P. E. Hopkins, *Phys. Rev. B* **93**,  
488 024201 (2016).
- 489 <sup>19</sup> W.-L. Ong, S. Majumdar, J. A. Malen, and A. J. H. McGaughey, *The Journal of Physical*  
490 *Chemistry C* **118**, 7288 (2014).
- 491 <sup>20</sup> W.-L. Ong, S. M. Rupich, D. V. Talapin, A. J. H. McGaughey, and J. A. Malen, *Nat Mater*  
492 **12**, 410 (2013).
- 493 <sup>21</sup> M. D. Losego, I. P. Blitz, R. A. Vaia, D. G. Cahill, and P. V. Braun, *Nano Letters* **13**, 2215  
494 (2013).
- 495 <sup>22</sup> J. P. Feser, E. M. Chan, A. Majumdar, R. A. Segalman, and J. J. Urban, *Nano Letters* **13**,  
496 2122 (2013).
- 497 <sup>23</sup> J. C. Duda, P. E. Hopkins, Y. Shen, and M. C. Gupta, *Phys. Rev. Lett.* **110**, 015902 (2013).
- 498 <sup>24</sup> M. D. Losego, M. E. Grady, N. R. Sottos, D. G. Cahill, and P. V. Braun, *Nat Mater* **11**, 502  
499 (2012).
- 500 <sup>25</sup> P. E. Hopkins, M. Baraket, E. V. Barnat, T. E. Beechem, S. P. Kearney, J. C. Duda, J. T.  
501 Robinson, and S. G. Walton, *Nano Letters* **12**, 590 (2012).
- 502 <sup>26</sup> R. Y. Wang, R. A. Segalman, and A. Majumdar, *Applied Physics Letters* **89**, 173113 (2006).
- 503 <sup>27</sup> Z. Wang, J. A. Carter, A. Lagutchev, Y. K. Koh, N.-H. Seong, D. G. Cahill, and D. D. Dlott,  
504 *Science* **317**, 787 (2007).
- 505 <sup>28</sup> Z. Wang, D. G. Cahill, J. A. Carter, Y. K. Koh, A. Lagutchev, N.-H. Seong, and D. D. Dlott,  
506 *Chemical Physics* **350**, 31 (2008).
- 507 <sup>29</sup> P. J. O'Brien, S. Shenogin, J. Liu, P. K. Chow, D. Laurencin, P. H. Mutin, M. Yamaguchi,  
508 P. Keblinski, and G. Ramanath, *Nat Mater* **12**, 118 (2013).

- 509 <sup>30</sup> Y. Jin, C. Shao, J. Kieffer, K. P. Pipe, and M. Shtein, *Journal of Applied Physics* **112**, 093503  
510 (2012).
- 511 <sup>31</sup> See Supplemental Material at [] for information on experimental and analytical details.
- 512 <sup>32</sup> T. Tynell and M. Karppinen, *Thin Solid Films* **551**, 23 (2014).
- 513 <sup>33</sup> J.-P. Niemelä and M. Karppinen, *Dalton Trans.* **44**, 591 (2015).
- 514 <sup>34</sup> D. G. Cahill, *Review of Scientific Instruments* **75**, 5119 (2004).
- 515 <sup>35</sup> A. J. Schmidt, X. Chen, and G. Chen, *Rev Sci Instrum* **79**, 114902 (2008).
- 516 <sup>36</sup> P. E. Hopkins, J. R. Serrano, L. M. Phinney, S. P. Kearney, T. W. Grasser, and C. T. Harris,  
517 *Journal of Heat Transfer* **132**, 081302 (2010).
- 518 <sup>37</sup> G. Tas and H. J. Maris, *Phys. Rev. B* **49**, 15046 (1994).
- 519 <sup>38</sup> V. P. Elena R. Dobrovinskaya, Leonid A. Lytvynov, *Sapphire: Material, Manufacturing, Appli-*  
520 *cations*, 1st ed. (Springer, 2009).
- 521 <sup>39</sup> J. Alvarez-Quintana, E. Martínez, E. Pérez-Tijerina, S. A. Pérez-García, and J. Rodríguez-  
522 Viejo, *Journal of Applied Physics* **107**, 063713 (2010).
- 523 <sup>40</sup> C. Ho, *Thermal conductivity of the elements : a comprehensive review* (New York : American  
524 Chemical Society and the American Institute of Physics for the National Bureau of Standards,,  
525 1975).
- 526 <sup>41</sup> C. Klingshirn, A. Waag, A. Hoffmann, and J. Geurts, *Zinc Oxide: From Fundamental Properties*  
527 *Towards Novel Applications*, Vol. 120 (Springer, 2010).
- 528 <sup>42</sup> R. M. Costescu, M. A. Wall, and D. G. Cahill, *Phys. Rev. B* **67**, 054302 (2003).
- 529 <sup>43</sup> J. C. Duda, P. M. Norris, and P. E. Hopkins, *Journal of Heat Transfer* **133**, 074501 (2011).
- 530 <sup>44</sup> J. Serrano, F. Manjón, A. Romero, A. Ivanov, M. Cardona, R. Lauck, A. Bosak, and M. Krisch,  
531 *Phys. Rev. B* **81**, 174304 (2010).
- 532 <sup>45</sup> J. Ravichandran, A. K. Yadav, R. Cheaito, P. B. Rossen, A. Soukiassian, S. J. Suresha, J. C.  
533 Duda, B. M. Foley, C.-H. Lee, Y. Zhu, A. W. Lichtenberger, J. E. Moore, D. A. Muller, D. G.  
534 Schlom, P. E. Hopkins, A. Majumdar, R. Ramesh, and M. A. Zurbuchen, *Nat Mater* **13**, 168  
535 (2014).
- 536 <sup>46</sup> P. M. Norris, N. Q. Le, and C. H. Baker, *Journal of Heat Transfer* **135**, 061604 (2013).
- 537 <sup>47</sup> M. N. Luckyanova, J. Garg, K. Esfarjani, A. Jandl, M. T. Bulsara, A. J. Schmidt, A. J. Minnich,  
538 S. Chen, M. S. Dresselhaus, Z. Ren, E. A. Fitzgerald, and G. Chen, *Science* **338**, 936 (2012).
- 539 <sup>48</sup> W. A. Little, *Canadian Journal of Physics* **37**, 334 (1959).



540 <sup>49</sup> I. M. Khalatnikov, Journal of Experimental and Theoretical Physics (Zhurnal Eksperimentalnoi  
541 i Teoreticheskoi Fiziki) **22**, 687 (1952).

542 <sup>50</sup> G. Chen and T. Zeng, Microscale Thermophysical Engineering **5**, 71 (2001).

543 <sup>51</sup> R. M. Costescu, D. G. Cahill, F. H. Fabreguette, Z. A. Sechrist, and S. M. George, Science  
544 **303**, 989 (2004).

545 <sup>52</sup> Y. K. Koh, Y. Cao, D. G. Cahill, and D. Jena, Advanced Functional Materials **19**, 610 (2009).

546 <sup>53</sup> P. E. Hopkins, J. C. Duda, C. W. Petz, and J. A. Floro, Phys. Rev. B **84**, 035438 (2011).

547 <sup>54</sup> J. C. Duda and P. E. Hopkins, Applied Physics Letters **100**, 111602 (2012).

548 <sup>55</sup> P. E. Hopkins, L. M. Phinney, J. R. Serrano, and T. E. Beechem, Phys. Rev. B **82**, 085307  
549 (2010).

550 <sup>56</sup> P. Sundberg and M. Karppinen, Beilstein Journal of Nanotechnology **5**, 1104 (2014).

551 <sup>57</sup> A. J. Karttunen, T. Tynell, and M. Karppinen, The Journal of Physical Chemistry C **119**,  
552 13105 (2015).

553 <sup>58</sup> J. C. Duda, C. B. Saltonstall, P. M. Norris, and P. E. Hopkins, The Journal of Chemical Physics  
554 **134**, 094704 (2011).

555 <sup>59</sup> T. Meier, F. Menges, P. Nirmalraj, H. Hölscher, H. Riel, and B. Gotsmann, Phys. Rev. Lett.  
556 **113**, 060801 (2014).

557 <sup>60</sup> D. Segal, A. Nitzan, and P. Hänggi, The Journal of Chemical Physics **119**, 6840 (2003).

558 <sup>61</sup> R. E. Jones, J. C. Duda, X. W. Zhou, C. J. Kimmer, and P. E. Hopkins, Applied Physics  
559 Letters **102**, 183119 (2013).